Wang, R. et al. (2013). Montmorillonite modified by CNx supported Pt for methanol oxidation.
International Journal of Hydrogen Energy, 38: 10381 – 10388
http://dx.doi.org/10.1016/j.ijhydene.2013.06.032



# Montmorillonite modified by CNx supported Pt for methanol oxidation

Rongfang Wang, Tianbao Zhou, Xiaoli Qiu, Hui Wang, Qizhao Wang, Hanqing Feng, Vladimir Linkov and Shan Ji

**Abstract**

A composite support based on nature clay, i.e. montmorillonite (MMT), shows great promise as support materials for Pt electrocatalyst for the methanol oxidation reaction in fuel cell anodes. The reported composite support ($CN_X$-MMT) was prepared via carbonizing MMT which was covered by N-contented polymer. X-ray diffraction and transmission electron microscopy results showed that Pt nanoparticles can be well-dispersed on the composite support with highly dispersed tiny crystal Pt nanoparticles. Cyclic voltammetry measurements showed that the Pt/$CN_X$-MMT has the enhanced electrocatalytic activity in methanol oxidation reaction. The developed Pt catalyst supported on new composite support is catalytically more active for methanol electrooxidation than Pt supported on the conventional carbon support and shows good stability, offering promising potential for application of MMT as support for fuel cell electrocatalysis.

## 1. Introduction

Direct methanol fuel cells (DMFCs) are considered as a promising candidate for future mobile and transport applications due to their high efficiency and low emissions. Platinum is used as the main element for DMFCs because it is highly active at low temperature and easily reactive with the hydrogen, alcohols and oxygen intermediates to generate the final products [1e3]. However, there are several challenges which constraint the commercialization of DMFCs, such as, insufficient durability and high cost [4e7]. The corrosion of conventional carbon support has been identified as a major contributor to the low durability for Pt-based electrocatalysts [8]. The stability of the supports for Pt-based electrocatalysts must be significantly increased to make this technology economically viable.

Recently, to develop the new support for immobilizing metal nanoparticles as electrocatalysts for fuel cells has become a subject of growing interest. One of the approaches it to develop new supports based on porous silica due to their large surface areas, high stability and uniform pore distribution. Eswaramoorthi and Dalai [9] synthesized Santa Barbara amorphous material-15-support for PdeZn

nanoparticles, which was used as catalyst to produce $H_2$ from $CH_3OH$ by partial oxidation and steam reforming. The initial results showed that porous silica show great promise as a catalyst support for fuel cell applications. However, the low conductivity of silica materials pose major barrier to the replacement of conventional carbon support by porous silica. An efficient way to improve the electric conductivity and stability is to introduce nitrogen doped carbon onto the surface of supports through the effect of N-doping on the surface to improve physicochemical properties, electron transfer and nanostructure of the catalysts [10e16]. Zhou et al. [10] prepared core/shell carbon fibers with N-doping on the surface, which provides significant improvements in their catalytic performance as catalyst supports for methanol electrochemical oxidation. Wang et al. [13] developed a N-doped carbon/$Fe_3O_4$ as support to immobilize Pd for catalytic oxidation of formic acid. The experimental results showed that N-doped carbon/ $Fe_3O_4$ support exhibited higher activity and better stability for oxidation of formic acid than both commercial Pd/C and Pt/C catalysts.

The pore-like structure of MMT, natural clay, contains layers made up of two tetrahedral silica sheets fused to an edge-shared octahedral sheet of alumina [17]. The application of MMT as support of catalysts has been reported. For example, the catalyst, $MoO_3$ supported on MMT, exhibited a higher activity in methanol oxidation to formaldehyde, probably due to the fact that impregnation ensures better dispersion of $MoO_3$ in MMT [18]. Intercalated MMT catalysts with low loaded Pt nanoparticles showed comparable selectivity of the product cinnamyl alcohol at very high conversion in the liquid phase hydrogenation of cinnamaldehyde at different pressures of hydrogen even at room temperature and at moderate pressure [19]. In electrochemical area, The MMT composite membranes showed a high selectivity and power density due to low methanol permeability [20]. Furthermore, after MMT modified the composite membranes contain functionalized MMT was endow with the high proton conductivity, low methanol permeability and suitable thermal stability leading to drastic reduction of methanol crossover and lower loss of conductivity properties [21e25].

Compared with porous carbon materials, MMT is much cheaper due to its accessibility and abundance. MMT is also chemical inert and environmentally friendly, which makes it a potential candidate as a promising support for fuel cell applications. Unfortunately, the electrical conductivity of MMT is quite low, which hinders its practical application as electrocatalyst support for fuel cells. In this study, a N-doped carbon/ MMT ($CN_X$-MMT) has been prepared by carbonizing polyaniline (PA) on the surface of MMT to improve its conductivity, which makes MMT suitable for using as support materials for electrocatalysts. Subsequently, Pt nanoparticles were deposited on the surface of $CN_X$-MMT, and its morphology and electrocatalytic performance were investigated.

## 2. Experimental

### *2.1 Preparation of $CN_x$-MMT*

15.0 g of MMT (Toksun, Xinjiang) was introduced to a 500 mL flask, and then 300 mL of 3 mol $L^{-1}$ HCl solution was added to the flask. The solution was stirred for 24 h, filtered and rinsed with ultrapure water. The acid-treated MMT was then dried at 60 $^{0}$ C in vacuum oven. Polymerization of aniline on MMT was carried out in a solution containing $(NH_4)_2S_2O_8$ as oxidant. A 150 mL of HCl solution containing MMT (0.5 g) and $(NH_4)_2S_2O_8$ (1.5 g) was sonicated at room temperature for 15 min. 1.0 g of anline was added to above solution and stirred at 0 $^{0}$ C for 24 h. After that, the product was filtered and rinsed with ultrapure water until the pH of solution is ca. 7. The obtained powder, MMT-polyaniline (PA-MMT), was dried at 60 $^{0}$ C for 12 h in vacuum oven. Carbonization of PA-MMT was carried out via the decomposition of polyaniline at high temperature, and the procedure was as follows: PA-MMT was placed in a quartz tube furnace and heated to 800 $^{0}$ C with a heating rate of 5 $^{0}$ C $min^{-1}$ under $N_2$ atmosphere and kept at 800 $^{0}$ C for 2 h. After the furnace was cooled to room temperature, a black powder, $CN_X$-MMT, was obtained.

### *2.2. Preparation of Pt/$CN_x$-MMT*

Before Pt nanoparticles were deposited on the surface of $CN_X$- MMT, the obtained $CN_X$-MMT was immersed in acetone and kept at 60 $^{0}$ C for 6 h in an oil bath. The acetone washed $CN_X$-MMT powder was rinsed with ultrapure water, and then added to a mixture of $HNO_3eH_2O_2$ (2 mol $L^{-1}$ $HNO_3$, 3 wt% $H_2O_2$) and stirred for 24 h in a dark environment. After that, the obtained product was rinsed with ultrapure water and dried at 60 $^{0}$C in a vacuum oven. Pt catalysts (loading ca. 20 wt %) supported on $CN_X$-MMT were prepared by an ethylene glycol (EG) solution method. $H_2PtCl_6$ (66.4 mg) was dissolved in 30 mL of EG in a flask. The pH of the system was adjusted to 10 by adding 5 wt% of KOH/EG solution. The powder of $CN_X$-MMT (100 mg) was added to the $H_2PtCl_6$ solution and then heated to 160 $^{0}$ C for 6 h. The resulting catalyst (Pt/$CN_X$-MMT) was filtered, washed with ultrapure water and dried in vacuum oven. Pt/C catalyst used in this work were purchased from Johnson Matthey Company (20% Pt, particles are 3e6 nm).

### *2.3. Morphological characterizations*

X-ray diffraction (XRD) was obtained by a Shimadzu XD-3A (Japan), using filtered Cu Ka radiation (40 kV, 40 mA). Scanning electron microscope images were obtained by a Hitachi S-2400 (Japan). Transmission electron microscopy (TEM) coupled with the energy dispersive X-ray analysis (EDX) technique and scanning electron microscope (SEM) measurements were carried out on a JEM-2010 (Japan) and a Hitachi S-2400 Electron Microscope (Japan), respectively. Elemental Analysis was measured by organic elemental analyzer (Thermo

Flash2000). The chemical compositions of Pt/$CN_X$-MMT catalyst were determined using an IRIS advantage inductively coupled plasma atomic emission spectroscopy (ICP-AES) system (Thermo, America).

### *2.4. Electrochemical characterizations*

The electrochemical measurements of catalysts were performed using an electrochemical work station (CHI650D). A conventional three-electrode electrochemicall cell was used for the measurements, including a platinum wire as the counter electrode as the reference electrode, and a glassy carbon electrode (5 mm in diameter) as the working electrode. A thin film electrode was prepared as follows: 5 mg of catalyst was dispersed ultrasonically in 1 mL of Nafion/ethanol (0.25% Nafion). 8 mL of the dispersion was transferred onto the glassy carbon disc using a pipette, and then dried in the air. Before each measurement, the solution was purged with high-purity $N_2$ for at least 30 min to ensure the gas saturated. All the tests were carried out at ambient temperature.

The practical composition of $CN_X$-MMT was evaluated by both EDX and elemental analysis. The analytical results indicate that $CN_X$-MMT consists of: N (10.5 wt%), C (51.3 wt%), S (0.3 wt %) from $(NH_4)_2S_2O_8$ and the remainder MMT. The EDX (Fig. 1) spectrum of $CN_X$-MMT identifies the presence of C, N, O, Si and Al elements. Other elements, such as Fe and Mg, are not present, maybe due to the too low content. The evaluated content of $Al_2O_3$ is ca. 0.85 wt% of MMT.

Fig. 2a presents the typical SEM image of MMT. It is observed that the acid-treated MMT with very rough surface appears irregular blocky morphology, which is similar to the reported morphology [26]. The morphology of the polymerization of PA on MMT is showed as Fig. 2b. Here, no separated MMT block is observed and PA-MMT clearly aggregates into clumps with very rough surface morphology since the PA encapsulation of MMT. After the carbonizing, $CN_X$-MMT shows a coral-shape in Fig. 2c. In the case of the composite, a separated vague $CN_X$-MMT block could be observed, and the coalesced others do not appear the morphology of MMT. It is believed that the graphene planar sheets are formed on the surface of the MMT block, resulting in the fact that the morphology of MMT is masked by PA.

We performed scanning transmission electron microscopy TEM and EDX line scanning analyses to reveal the structure of Fig. 1 e EDX spectrum of the MMT-$CN_X$ sample. $CN_X$-MMT composite, and TEM characterization is presented as Fig. 2d and e. From Fig. 2d, a hetero-structure can be clearly observed from the contrast, suggesting that the carbon layers are formed on the surface of MMT. The compositional line profile taken from the fringe of a block in Fig. 2e indicates that carbon surface is deposited on the MMT substrate (Fig. 2g andh). These results demonstrate the successful preparation of the hetero-structure consisting of MMT as a substrate and a surface of carbon. The carbon layer is uniformly formed on the

surface of MMT, which can provide an electronic conductive layer on the MMT. This carbon layer can offset the low electrical conductivity of MMT and make this $CN_X$-MMT suitable for as support for electrocatalysts.

XRD analysis was carried out to investigate the crystal structures of MMT and $CN_X$-MMT, which are shown in Fig. 3. The XRD pattern of MMT in Fig. 3a shows the typical XRD peaks of quartz at 2q of $20.7^0$ and $26.6^0$ , along with other weak reflections [27,28]. This implies that the octahedral crystal structure of MMT is destroyed by the acid solution, which is attributed to the dissolution of octahedral cations (e.g. $Mg^{2þ}$, $Al^{3þ}$, and $Fe^{3þ}$) in MMT crystal structure [26]. Nonetheless, the destruction to the crystal structure of MMT is not complete because a broad (001) peak was present in Fig. 3b. In the case of $CN_X$-MMT (see Fig. 3a), a broad diffraction peak in the range of $20e25^0$, ascribed to the plane (200) of carbon [29], appears. In addition, the typical diffraction peaks of quartz do not change for the position. However, the octahedral structure of MMT is completely destroyed by the heat-treatment, which is confirmed from the disappear of (001) peak in Fig. 3b [30]. This phenomenon is consistent with the Wu's report [31]. XRD characterizations suggest the hetero-structure composite is formed from PA-MMT (Fig. 3).

To investigate the support effect of $CN_X$-MMT, we choose Pt nanoparticles to deposited on the surface of $CN_X$-MMT for Pt metal is the most widely use in electrocatalysts. The crystal structure of Pt/$CN_X$-MMT was characterized through XRD, which is also shown in Fig. 3a. The typical diffraction peaks of MMT located at $2q ¼ 21^0$ and $27^0$ could be clearly observed after the carbonization of polyaniline at high temperature and Pt deposited on its surface. The XRD results show that the structure of MMT is stable to the process of preparing Pt/$CN_X$-MMT. The characteristic peaks of Pt (fcc) at around $27^0$, $39^0$ , $46^0$ and $67^0$ attributed to the Pt (004), (111), (200) and (220) planes, respectively, are observed. The XRD of Pt/$CN_X$-MMT shows that Pt (fcc) particles are formed on the $CN_X$-MMT.

TEM image of Pt/$CN_X$-MMT (Fig. 4a) shows that the Pt nanoparticles are well-dispersed on the surface of the $CN_X$-MMT support. TEM image reveals that the carbon layer and MMT appeared well attached, and good contact between the two supports could therefore facilitate the transport of fuel, oxidant and electrons. The agglomeration of the nanoparticles on the surface of carbon is observed in Pt/$CN_X$-MMT. Size distribution of Pt/$CN_X$-MMT is depicted in Fig. 4b, which shows that the average size of Pt nanoparticles deposited on the surface of $CN_X$-MMT support is ca. 5.4 nm. Pt loading by ICP is ca. 20 wt% of the catalyst.

Fig. 5 depicts the cyclic voltammograms (CVs) of Pt/C and Pt/$CN_X$-MMT catalysts in 0.5 mol $L^{-1}$ $H_2SO_4$ solution in the voltage range from -0.2 to 1.0 V (vs. Ag/AgCl) at

a scan rate of 50 mV $s^{-1}$ at the room temperature. The three characteristic peaks of polycrystalline Pt, i.e. hydrogen adsorption/desorption peaks in low potential region, oxide formation/stripping wave/peak in high potential region and a flat double layer in between, are observed in the CV curves of both catalysts.

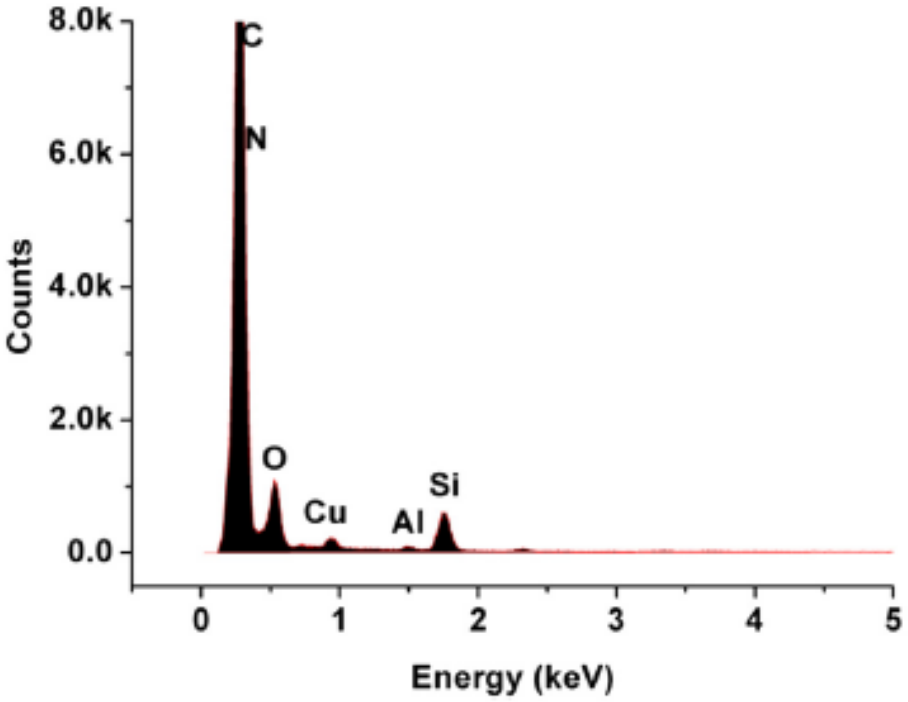


**Fig. 1 – EDX spectrum of the MMT-$CN_x$ sample.**

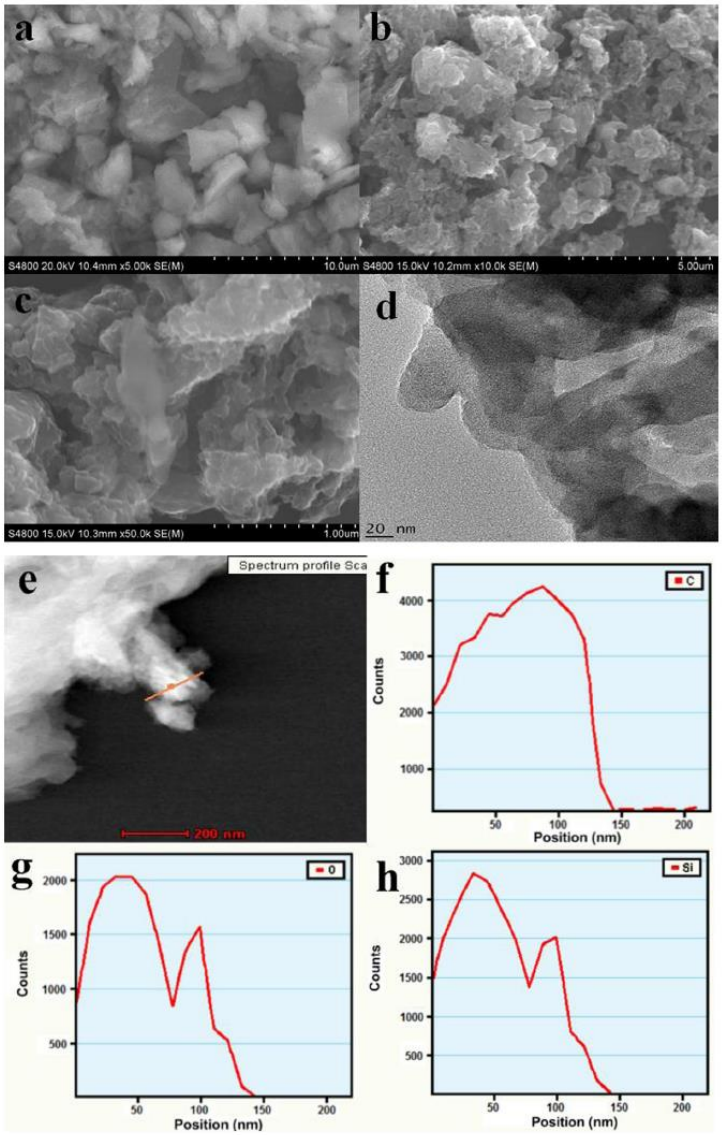


Fig. 2 – SEM images of MMT (a), PA-MMT (b), $CN_x$-MMT (c), TEM images of $CN_x$-MMT (d and e); and EDX line scanning spectra for C (f), O (g) and Si (h).

In the potential range from -0.2 to 0.1 V, three hydrogen desorption peaks are observed at -0.1, -0.01, 0.03 V, corresponding to the catalytic effects of Pt (111), Pt (110), Pt (100) planes, respectively [32]. The electrochemically accessible area of $Pt/CN_X$-MMT is significantly greater than that of Pt/C in the light of the double-layer behavior, which would facilitate access of solvated and charged ions on N-doped carbon on $CN_X$-MMT support [12,29,33]. In addition, the peak of Pt (100) in the CV of $Pt/CN_X$-MMT is much higher than that of Pt/C, which indicates that the Pt (100) plane in the catalyst of $Pt/CN_X$ is much more than conventional Pt/C catalyst. Xia et al. [34] reported that higher ratio of Pt (100) and Pt (111) results in high electrocatalytic activity. Based on the CV results, it is expected that the $Pt/CN_X$-MMT may show higher electro-catalytic activity than Pt/C.

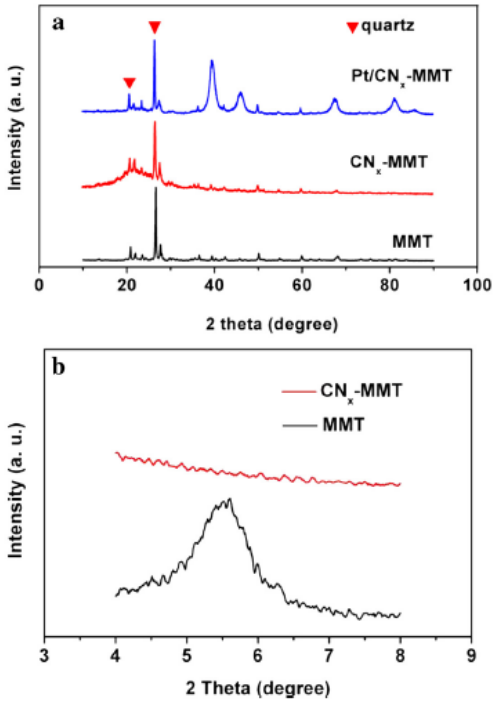


Fig. 3 – (a): XRD patterns of MMT, $CN_x$-MMT and Pt/$CN_x$-MMT, 2$\theta$: 10–90°; (b): XRD patterns of MMT and $CN_x$-MMT, 2$\theta$: 4–8°.

The electrochemical active surface area (ECSA) value is able to provide value information about the amount of electrochemically active sites on a mass basis of the precious metal and is also a crucial parameter for comparison of different electrocatalytic support. ECSA of Pt/C and Pt/$CN_X$-MMT were calculated by the following equation [35]: ECSA ¼ Q H=½210 x Pt] where $Q_H$ ($cm^{-2}$) is the charge exchanged during the electroadsorption of hydrogen on Pt at the potential range of -0.13 to þ0.2 V (vs. Ag/AgCl), 210 is the charge (mC $cm^{-2}$) required to oxidize a monolayer of hydrogen on the Pt surface and Pt is the Pt loading on the electrode. The ECSA of Pt/C and Pt/$CN_X$-MMT are 21.2 and 36.6 $m^2$ $g^{-1}$, respectively. The ECSA of Pt/$CN_X$-MMT is 1.73 times higher than that of Pt/C, which means more electrochemically active sites available on the surface of Pt deposited on $CN_X$-MMT support.

CVs in terms of specific activity (Fig. 6) were carried out to demonstrate the improved specific activity of $CN_X$-MMT to methanol oxidation reaction. The CVs of Pt/C and Pt/$CN_X$-MMT were conducted in a mixture of 0.5 mol $L^{-1}$ $CH_3OH$ þ 0.5 mol $L^{-1}$ $H_2SO_4$ solution at 50 mV $s^{-1}$ at room temperature. The onset potential and the forward peak potential of Pt/$CN_x$-MMT and Pt/C catalyst, and other values reported in the similar litera- tures [36e39] are listed in Table 1.

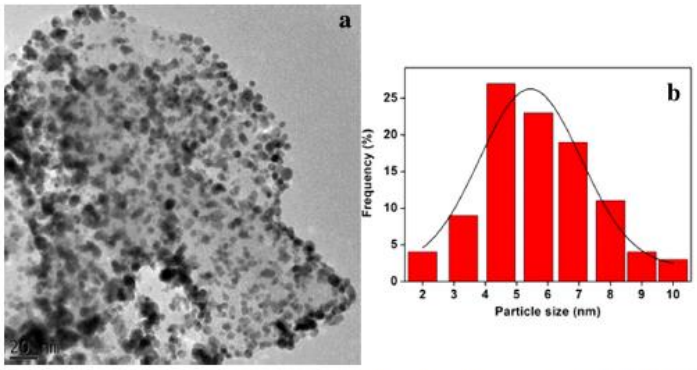


Fig. 4 – TEM image of $Pt/CN_x$-MMT (a) and particle size distribution of $Pt/CN_x$-MMT (b).

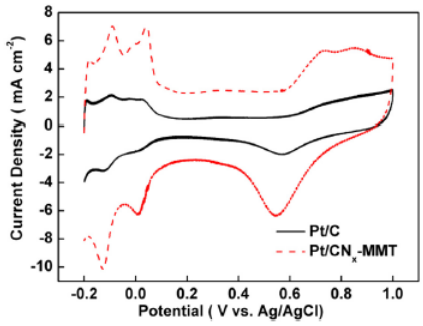


Fig. 5 – Cyclic voltammograms of Pt/C and $Pt/CN_x$-MMT catalysts in 0.5 mol $L^{-1}$ $H_2SO_4$ solution run at 50 mV $s^{-1}$ at room temperature.

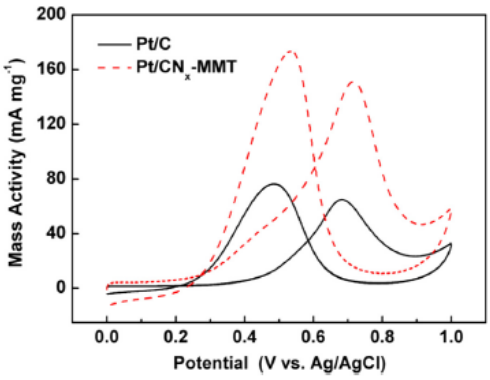


Fig. 6 – Cyclic voltammograms of Pt/C and $Pt/CN_x$-MMT catalysts in 0.5 mol $L^{-1}$ $CH_3OH$ + 0.5 mol $L^{-1}$ $H_2SO_4$ solution run at 50 mV $s^{-1}$ at room temperature.

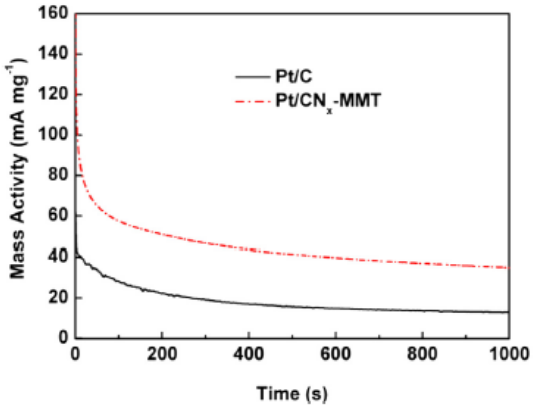


Fig. 7 – Chronoamperometric curves of Pt/C and Pt/$CN_x$-MMT for methanol oxidation, at a constant potential of +0.5 V *vs.* Ag/AgCl and at room temperature.

The onset potential of methanol oxidation at Pt/$CN_X$-MMT catalyst is lower than that of Pt/C catalyst, while the forward peak potential of Pt/$CN_X$- MMT catalyst positively shifts compared with Pt/C catalyst. The peak oxidation current of Pt/$CN_X$-MMT is 2.3 times higher than that of Pt/C. In addition, it should be noted that the onset potential of Pt/$CN_X$-MMT catalyst is also negative than those of previously reported [36e39]. These findings can be attributed to an increased number of catalytically active sites toward the methanol oxidation on the surface of Pt/$CN_X$-MMT.

The ratio of the forward anodic peak current ($I_f$) to the reverse anodic peak current ($I_b$) can be used to describe the catalyst tolerance to accumulation of carbonaceous species. A higher ratio indicates more effective removal of the poisoning species on the catalyst surface. The $I_f/I_b$ ratios of Pt/$CN_X$-MMT and Pt/C are 0.87 and 0.84, respectively, which is given in Table 1. The $I_f/I_b$ ratio of Pt/$CN_X$-MMT is close the values reported in Ref. [39] because oxide in the two catalyst is covered by carbon layer. On the contrary, The $I_f/I_b$ ratio of Pt/$CN_X$-MMT is clearly lower than Pt/$SiO_2$ [36], Pt/$V_2O_5$eC [37]. The results maybe caused by that oxide presented on the surface would facilitate remove the poisoning species. The $I_f/I_b$ ratio of Pt/C (0.84) is close those reported in previously literatures [37,38], indicating that the value tested by us is normal.

Chronoamperometric curves of Pt/C and Pt/$CN_X$-MMT were obtained to determine the effect of CO adsorption during the methanol oxidation reaction. By keeping the electrode at a constant potential of 0.5 V (*vs.* Ag/AgCl) at room temperature, methanol oxidation takes place on the active sites of catalyst. Fig. 7 shows the chronoamperometric curves of Pt/C and Pt/ $CN_X$-MMT for the methanol oxidation. The CO intermediates, such as $CO_{ad}$, formed during MOR, can cover the active sites of Pt nanoparticles, and further results in decay of electrocatalytic activity. The long term poisoning rates of Pt/C and Pt/ $CN_X$-MMT are calculated by measuring the ratio

of the current at 1000 s ($I_{1000}$) and 100 s ($I_{100}$). The ratios of $I_{1000}/I_{100}$ for Pt/C and Pt/$CN_X$-MMT are found to be 26.1% and 52.5%, respectively. In this manner, Pt/$CN_X$-MMT maintains a higher specific activity than Pt/C for the oxidation of methanol during chronoamperometry.

**Table 1 – Comparison of electrochemical performance for methanol oxidation between as-prepared Pt/$CN_x$-MMT catalyst and silica supported Pt catalysts reported in literatures.**

| Catalyst | Onset potential[f] | Forward peak potential[f] | $I_f/I_b$ |
|---|---|---|---|
| Pt/$CN_x$-MMT | 0.13 | 0.72 | 0.87 |
| Pt/C | 0.27 | 0.68 | 0.84 |
| Pt/$SiO_2$ [36],[a] | −0.18[b] | 0.158[b] | 1.3 |
| Pt/C (J. M.) [37],[c] | 0.31 | 0.76 | 0.9 |
| Pt/$V_2O_5$–C [37],[c] | 0.21 | 0.811 | 1.06 |
| Pt/$TiO_2$@C-900 [38],[d] | 0.25 | 0.77 | 0.62 |
| Pt/Vulcan XC-72R [38],[d] | 0.25 | 0.72 | 0.49 |
| Pt/$C_{40}$–$CeO_2$ [39],[e] | 0.35 | 0.71 | 0.86 |

a Scan rate: 10 mV $s^{-1}$, electrolyte: 0.5 mol $L^{-1}$ methanol + 0.5 mol $L^{-1}$ $H_2SO_4$.
b Reference electrode Ag/$Ag_2SO_4$.
c Scan rate: 50 mV $s^{-1}$, electrolyte: 1 mol $L^{-1}$ methanol + 1 mol $L^{-1}$ $H_2SO_4$.
d Scan rate: 50 mV $s^{-1}$, electrolyte: 2 mol $L^{-1}$ methanol + 0.5 mol $L^{-1}$ $H_2SO_4$.
e Scan rate: 50 mV $s^{-1}$, electrolyte: 0.5 mol $L^{-1}$ methanol + 0.5 mol $L^{-1}$ $H_2SO_4$.
f Unit: V *vs.* Ag/AgCl.

## 4. Conclusions

This work showed that carbonization of N-contented polymers on the surface of natural clays provides an efficient measure for preparing supports for fuel cell electrocatalysts. Well-dispersed Pt nanoparticles were successfully synthesized on the surface of $CN_X$-MMT and were found to have MOR specific activity 2.3 times greater than that of Pt/C catalyst. From the electrochemical studies, Pt nanoparticles deposited on the composite support yielded larger ECSA values than conventional carbon one. CV and CO-stripping results proved that Pt/$CN_X$-MMT catalysts were catalytically more active and stable toward MOR than conventional Pt/C. Further work is underway to determine which aspects of these electrocatalysts mainly result in their high activity and stability under fuel cell operating conditions.

## Acknowledgments

This work was financially supported by the National Natural Science Foundation of China (21163018) and the National Science Foundation for Post-Doctoral Scientists of China (20110490847, 2012T50587).

**References**

[1] Alayoglu S, Nilekar AU, Mavrikakis M, Eichhorn B. RuePt core-shell nanoparticles for preferential oxidation of carbon monoxide in hydrogen. Nat Mater 2008;7:333e8.
[2] Jha N, Imran Jafri R, Rajalakshmi, Ramaprabhu. Graphene- multi walled carbon nanotube hybrid electrocatalyst support material for direct methanol fuel cell. Int J Hydrogen Energy 2002;47:3777e85.
[3] Wang J, Yin G, Liu H, Li R, Flemming RL, Sun X. Carbon nanotubes supported PteAu catalysts for methanol-tolerant oxygen reduction reaction: a comparison between Pt/Au and PtAu nanoparticles. J Power Sources 2009;194:668e73.
[4] Wang Y-J, Wilkinson DP, Zhang J. Noncarbon support materials for polymer electrolyte membrane fuel cell electrocatalysts. Chem Rev 2011;111:7625e51.
[5] Esposito DV, Hunt ST, Stottlemyer AL, Dobson KD, McCandless BE, Birkmire RW, et al. Low-cost hydrogen- evolution catalysts based on monolayer platinum on tungsten monocarbide substrates. Angew Chem Int Ed 2010;49:9859e62.
[6] Fu Z, Huang QM, Xiang XD, Lin YL, Wu W, Hu SJ, et al. Mesoporous tungsten carbide-supported platinum as carbon monoxide-tolerant electrocatalyst for methanol oxidation. Int J Hydrogen Energy 2012;37:4704e9.
[7] Lv H, Mu S, Cheng N, Pan M. Nano-silicon carbide supported catalysts for PEM fuel cells with high electrochemical stability and improved performance by addition of carbon. Appl Catal B 2010;100:190e6.
[8] Donthu S, Cai M, Ruthkosky M, Halalay I. Carbonetitania composite substrates for fuel cell catalyst applications. Chem Commun 2009:4203e5.
[9] Eswaramoorthi I, Dalai AK. A comparative study on the performance of mesoporous SBA-15 supported Pd-Zn catalysts in partial oxidation and steam reforming of methanol for hydrogen production. Int J Hydrogen Energy 2009;34:2580e90.
[10] Zhou CF, Liu ZW, Du XS, Mitchell DRG, Mai YW, Yan YS, et al. Hollow nitrogen-containing core/shell fibrous carbon nanomaterials as support to platinum nanocatalysts and their TEM tomography study. Nanoscale Res Lett 2012;7:1e11.
[11] Vinayan BP, Nagar R, Rajalakshmi N, Ramaprabhu S. Novel platinumecobalt alloy nanoparticles dispersed on nitrogen- doped graphene as a cathode electrocatalyst for PEMFC applications. Adv Funct Mater 2012;22:3519e26.
[12] Wang R, Jia J, Li H, Li X, Wang H, Chang Y, et al. Nitrogen- doped carbon coated palygorskite as an efficient electrocatalyst support for oxygen reduction reaction. Electrochim Acta 2011;56:4526e31.
[13] Jia JC, Wang RF, Wang H, Ji S, Key J, Linkov V, et al. A novel structural design of CN(x)-Fe(3)O(4) as support to immobilize Pd for catalytic oxidation of formic acid. Catal Commun 2011;16:60e3.
[14] Fellinger TP, Hasche F, Strasser P, Antonietti M. Mesoporous nitrogen-doped carbon for the electrocatalytic synthesis of hydrogen peroxide. J Am Chem Soc 2012;134:4072e5.

[15] Lei Z, An L, Dang L, Zhao M, Shi J, Bai S, et al. Highly dispersed platinum supported on nitrogen-containing ordered mesoporous carbon for methanol electrochemical oxidation. Micropor Mesopor Mat 2009;119:30e8.
[16] Liu Y, Jin Z, Wang J, Cui R, Sun H, Peng F, et al. Nitrogen- doped single-walled carbon nanotubes grown on substrates: evidence for framework doping and their enhanced properties. Adv Funct Mater 2011;21:986e92.
[17] Sarier N, Onder E, Ersoy S. The modification of Na- montmorillonite by salts of fatty acids: an easy intercalation process. Colloid Surf A e Physicochem Eng Asp 2010;371:40e9.
[18] Klissurski D, Petridis D, Abadzhieva N, Hadjiivanov K. MOO, supported on montmorillonite type pillared clays: characterization, surface acidity and catalytic properties towards the oxidation of methanol. Appl Clay Sci 1996;10:451e9.
[19] Manikandan D, Divakar D, Rupa AV, Revathi S, Preethi MEL, Sivakumar T. Synthesis of platinum nanoparticles in montmorillonite and their catalytic behaviour. Appl Clay Sci 2007;37:193e200.
[20] Jung DH, Cho SY, Peck DH, Shin DR, Kim JS. Preparation and performance of a Nafion®/montmorillonite nanocomposite membrane for direct methanol fuel cell. J Power Sources 2003;118:205e11.
[21] Yang C- C. Fabrication and characterization of poly(vinyl alcohol)/montmorillonite/poly(styrene sulfonic acid) proton- conducting composite membranes for direct methanol fuel cells. Int J Hydrogen Energy 2011;36:4419e31.
[22] Gosalawit R, Chirachanchai S, Shishatskiy S, Nunes SP. Sulfonated montmorillonite/sulfonated poly(ether ether ketone) (SMMT/SPEEK) nanocomposite membrane for direct methanol fuel cells (DMFCs). J Membr Sci 2008;323:337e46.
[23] Chuang S-W, Hsu SL-C, Hsu C-L. Synthesis and properties of fluorine-containing polybenzimidazole/montmorillonite nanocomposite membranes for direct methanol fuel cell applications. J Power Sources 2007;168:172e7.
[24] Hasani-Sadrabadi MM, Emami SH, Moaddel H. Preparation and characterization of nanocomposite membranes made of poly(2,6-dimethyl-1,4-phenylene oxide) and montmorillonite for direct methanol fuel cells. J Power Sources 2008;183:551e6.
[25] Hasani-Sadrabadi MM, Dashtimoghadam E, Majedi FS, Kabiri K. Nafion®/bio-functionalized montmorillonite nanohybrids as novel polyelectrolyte membranes for direct methanol fuel cells. J Power Sources 2009;190:318e21.
[26] Yang D-S, Bhattacharjya D, Inamdar S, Park J, Yu J-S. Phosphorus-doped ordered mesoporous carbons with different lengths as efficient metal-free electrocatalysts for oxygen reduction reaction in alkaline media. J Am Chem Soc 2012;134:16127e30.
[27] Wu P, Du P, Zhang H, Cai C. Graphyne as a promising metal- free electrocatalyst for oxygen reduction reactions in acidic fuel cells: a DFT study. J Phys Chem C 2012;116:20472e9.